The West African monsoon dynamics, Part I: Intra-seasonal variability

Benjamin Sultan, Serge Janicot, Arona Diedhiou

The West African Monsoon Dynamics. Part I: Documentation of Intraseasonal Variability

BENJAMIN SULTAN AND SERGE JANICOT

LMD/IPSL, CNRS, Ecole Polytechnique, Palaiseau, France

ARONA DIEDHIOU

Laboratoire d'Etudes des Transferts en Hydrologie et Environnement, IRD, Grenoble, France

(Manuscript received 20 May 2002, in final form 9 January 2003)

ABSTRACT

Intraseasonal variability in the West African monsoon is documented by using daily gridded datasets of rainfall and convection, and reanalyzed atmospheric fields, over the period 1968–90. Rainfall and convection over West Africa are significantly modulated at two intraseasonal timescales, 10–25 and 25–60 day, leading to variations of more than 30% of the seasonal signal. A composite analysis based on the dates of the maximum (minimum) of a regional rainfall index in wet (dry) sequences shows that these sequences last, on average, 9 days and belong to a main quasiperiodic signal of about 15 days. A secondary periodicity of 38 days is present but leads to a weaker modulation. During a wet (dry) sequence, convection in the ITCZ is enhanced (weakened) and its northern boundary moves to the north (south), while the speed of the African easterly jet decreases (increases), the speed of the tropical easterly jet increases (decreases), and the monsoon flow becomes stronger (weaker), all these features being similar to the ones associated with interannual variability characterizing wet and dry years.

This modulation of convection at intraseasonal timescales is not limited to West Africa but corresponds to a westward-propagating signal from eastern Africa to the western tropical Atlantic. An enhanced monsoon phase is associated with stronger cyclonic activity in the low levels over the Sahel associated with stronger moisture advection over West Africa. Five days before the full development of the wet phase, a stronger cyclonic circulation at 20°E induces enhanced southerly winds along 25°E where convection enhances, while another westward-propagating cyclonic circulation is located at 0°. This atmospheric pattern is linked to the enhancement of the subsiding branch of the northern Hadley cell at 35°N, northerly advection of drier air over West Africa, and to increased dry convection in the heat low at 20°N. It propagates westward, leading to a zonally extended area of enhanced monsoon winds over West Africa consistent with the occurrence of the wet phase.

1. Introduction

Rainfall variability over West Africa has usually been analyzed either through mesoscale convective systems (MCS; Laing and Fritsch 1993, 1997; Hodges and Thorncroft 1997; Mathon and Laurent 2001), synoptic-scale easterly waves (Reed et al. 1977; Duvel 1990; Diedhiou et al. 1999), interannual timescale variability, and/or the decadal timescale of the long-term drought over the Sahel (Lamb 1978a,b; Folland et al. 1986; Rowell et al. 1995; Ward 1998; Rowell 2001; Janicot et al. 2001). Very few studies have investigated the West African monsoon through the intraseasonal timescale. Kiladis and Weickmann (1997) have shown some connections at the 6–30-day timescale between convection in the region 5°–15°N, 10°–20°E and moisture advection over West Africa during northern summer. More recently, Janicot and Sultan (2001) showed preliminary results of the evidence of specific intraseasonal variability in convective activity and low-level atmospheric circulation during the summer monsoon in West Africa. Grodsky and Carton (2001) showed that intraseasonal modulation of convection can also occur during northern spring in the ITCZ over the tropical Atlantic and they suggested a mechanism based on land–sea interactions.

A more detailed documentation of intraseasonal variability in the West African monsoon during northern summer is presented here. The data are described in section 2 and the summer of 1968 is shown in section 3 as an example of intraseasonal timescale rainfall fluctuations. In section 4 we describe the composite intraseasonal sequences of Sahel rainfall and we detail the associated atmospheric circulation patterns in section 5. Conclusions are given in section 6.

Corresponding author address: Dr. Serge Janicot, Laboratoire de Météorologie Dynamique, Ecole Polytechnique, 91128 Palaiseau Cedex, France.
E-mail: janicot@lmd.polytechnique.fr

2. Datasets

Independent datasets have been used to investigate the intraseasonal timescale variability of convection in the West African monsoon. Two of them describe rainfall and convection variability, two others are the European and U.S. reanalyses. They document the period 1968–90 and the subperiod 1979–90, which belong to a dry long-term sequence of the rainfall regime over West Africa compared to the long-term mean (Hastenrath 1995). We will show that all the results obtained with these different datasets coming from independent sources (rain gauge amounts, satellite measurements, atmospheric variables from radiosoundings, pibals, etc.), are very consistent.

a. The NCEP–NCAR reanalyses

The National Centers for Environmental Prediction–National Center for Atmospheric Research (NCEP–NCAR) have completed a reanalysis project with a current version of the Medium-Range Forecast (MRF) model (Kalnay et al. 1996). This dataset consists of a reanalysis of the global observational network of meteorological variables (wind, temperature, geopotential height, humidity on pressure levels, surface variables, and flux variables like precipitation rate) with a ''frozen'' state-of-the-art analysis and forecast system at a triangular spectral truncation of T62 to perform data assimilation throughout the period 1948 to the present. This makes it possible to circumvent problems of previous numerical weather prediction analyses due to changes in techniques, models, and data assimilation. Data are reported on a 2.5° × 2.5° grid every 6 h (0000, 0600, 1200, and 1800 UTC), on 17 pressure levels from 1000 to 10 hPa, which are good resolutions for studying synoptic weather systems. We used data covering the period 1 June–30 September, from 1968 to 1990, with one value per day by averaging the four outputs of each day.

b. The IRD daily rainfall

Daily rainfall amount at stations located on the West African domain 3°–20°N, 18°W–25°E have been compiled by the Institut de Recherche pour le Developpement (IRD), the Agence pour la Securite de la Navigation Aerienne en Afrique et a Madagascar (ASECNA), and the Comite Interafricain d'Etudes Hydrauliques (CIEH). These data are available for the period 1968–90, including more than 1300 stations from 1968 to 1980, and between 700 and 860 for the period 1981–90. These daily values were interpolated on the NCEP 2.5° × 2.5° grid, by assigning each station daily value to the nearest grid point and averaging all the values related to each grid point. They were also interpolated in time, related to NCEP daily wind fields since daily rainfall amounts were measured between 0600 of the day and 0600 local solar time (LST) of the following day. We applied a time lag of 12 h between the average time of the NCEP daily values (0900 UTC) and an approximated average time of ''daily'' precipitation over the West African continent (2100 LST; Duvel 1989), which indicates a maximum of high cloud coverage over land between 1800 and 0000 LST [Sow (1997) points out a maximum of half-hourly precipitation over the Senegal between 1700 LST and the end of the night, depending on the stations.] The greatest density of stations is located between the latitudes 5°–15°N. Data on latitudes 17.5°N can also be taken into account since 30–45 stations are available.

c. The NOAA/OLR dataset

Since 1974, launching polar orbital National Oceanic and Atmospheric Administration (NOAA) Television Infrared Observation Satellite (TIROS) satellites has made it possible to establish a quasi-complete series of twice-daily measures of outgoing longwave radiation (OLR), at the top of the atmosphere and at a resolution of 2.5° latitude–longitude (Gruber and Krueger 1984). The interpolated OLR dataset (Liebmann and Smith 1996) provided by the Climate Diagnostics Center has been used here. In tropical areas, deep convection and rainfall can be estimated through low OLR values. Local hours of the measures varied during the period 1979–90 between 0230 and 0730 in the morning and between 1430 and 1930 in the afternoon. Since the deep convection over West Africa has a strong diurnal cycle, the sample of daily OLR based on two values separated by 12 h is enough to get a daily average. Moreover this dataset has been already widely used for tropical studies.

d. The ECMWF Reanalyses (ERA-15)

The European Centre for Medium-Range Weather Forecasts (ECMWF) completed a first reanalysis project (ERA-15), which used a frozen version of their analysis-forecast system, at a triangular spectral truncation of T106 with 31 levels in the vertical, to perform data assimilation using data from 1979 to 1993 (Gibson et al. 1997). Compared to NCEP–NCAR reanalyses, there are 17 pressure levels from 1000 to 10 hPa, with an additional level at 775 and no level at 20 hPa. According to our objectives, daily data have been interpolated on the 2.5° × 2.5° NCEP–NCAR grid. The ERA-15 dataset has been used in comparison with the NCEP–NCAR dataset in order to evaluate the uncertainty of the wind fields produced by both reanalyses. Previous studies using these two reanalysis datasets already demonstrated their consistency over West Africa for describing both interannual and synoptic timescale variability, if we consider the period after 1968 (Diedhiou et al. 1999; Poccard et al. 2000; Janicot et al. 2001). The comparisons done here related to intraseasonal timescale variability also showed high consistency between these two data-

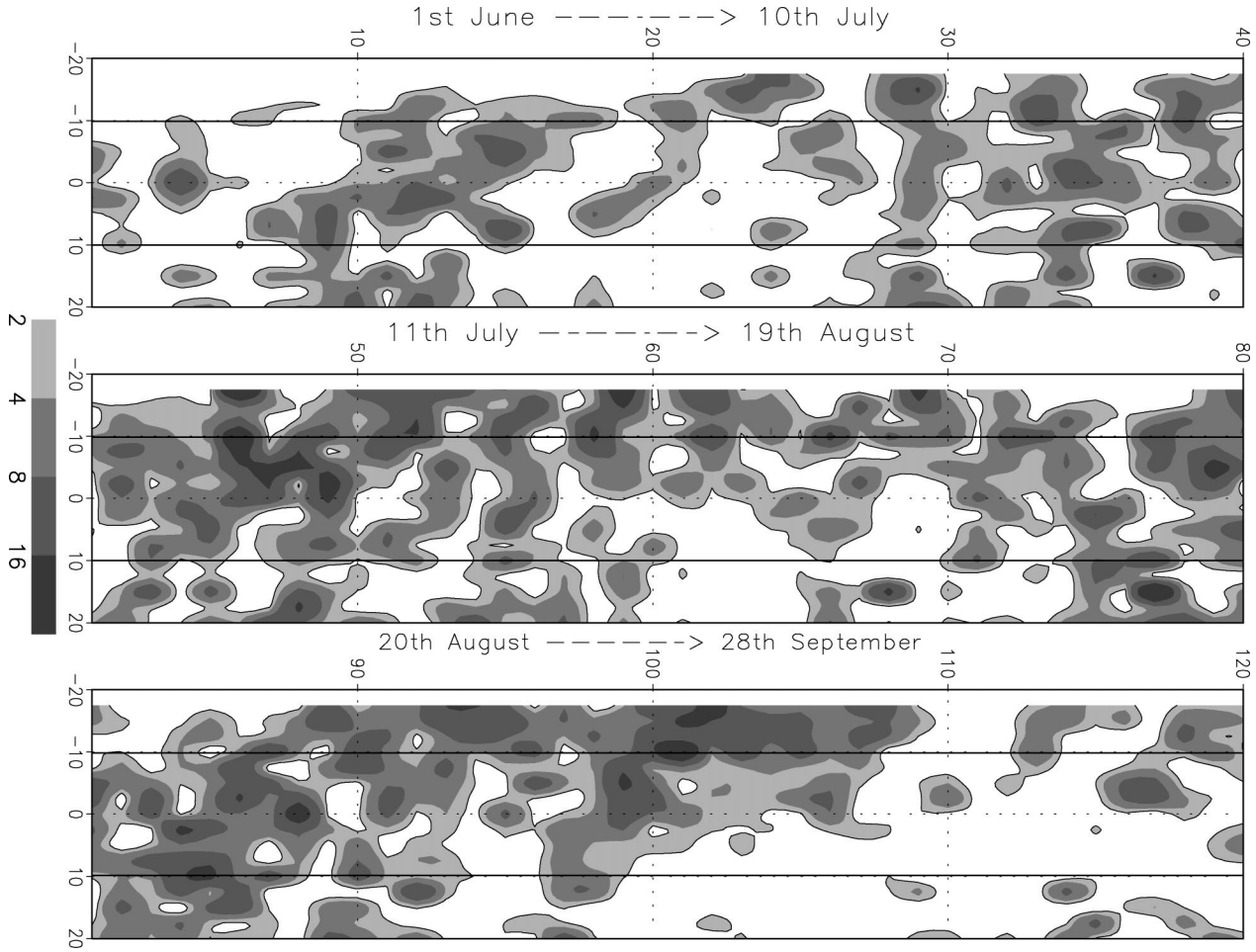

FIG. 1. Lon–time diagram of IRD daily rainfall (mm) averaged on the grid meshes at 12.5° and 15°N over West Africa for the summer of 1968 (1 Jun–28 Sep; i.e., 120 days). Vertical lines delineate longitudes 10°W and 10°E.

sets, so only results obtained from the NCEP–NCAR reanalysis, which covers the longest period 1968–90, will be shown in this paper.

3. Intraseasonal rainfall variability over West Africa in 1968

During the northern summer over West Africa, the ITCZ is centered along 10°N and extends in latitude over more than 10° (see, e.g., Sultan and Janicot 2000). The ITCZ consists of westward-traveling MCSs whose mean trajectories lie between 10° and 15°N (Mathon and Laurent 2001). Figure 1 shows a longitude–time diagram from 20°W to 20°E, of IRD daily rainfall averaged over the grid meshes at 12.5° and 15°N for the summer of 1968. Similar results have been obtained with computations performed at 10°N, the latitude of the mean rainfall maximum in the ITCZ (not shown). Different phases of high or low convective activity are clearly observed. During this year, the monsoon developed rapidly over West Africa from 27 June corresponding to the summer monsoon onset associated to an abrupt shift of the ITCZ (see Sultan and Janicot 2000; Sultan et al. 2003, for more details about the definition of the monsoon onset). This is characterized in Fig. 1 by the occurrence at the end of June of a band of higher rainfall simultaneously at all longitudes. Besides this monsoon onset sequence, main active monsoon phases can be detected, one before the onset, between 10 and 15 June, and several ones after the onset, one around mid-July (day 45), another one in the second half of August (centered on day 85), and a third around day 100 (8 September). Contrary to this, a less active convection sequence occurred, just before the monsoon onset in the second half of June (this decrease of convection is a recurrent character of the preonset stage; see Sultan and Janicot 2000; Le Barbé et al. 2002; Sultan et al. 2003), then around 1 August (day 60), and also around 20 September (day 110).

Figure 2a shows the time series from 1 June to 30 September 1968 of daily rainfall averaged over the grid meshes 12.5° and 15°N, from 10°W to 10°E (white bars). The black area behind the daily rainfall values represents the daily values of the seasonal rainfall cycle,

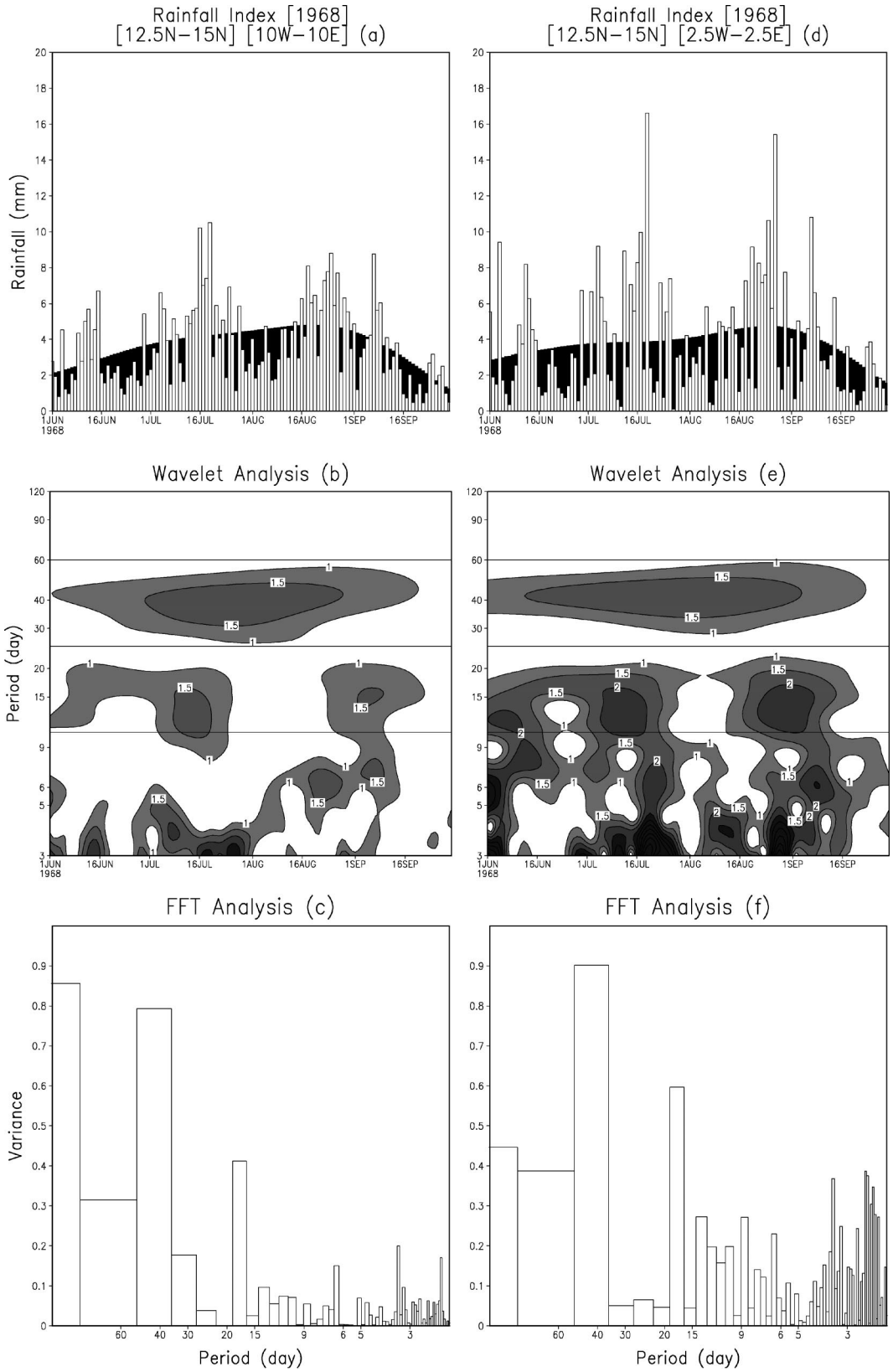

FIG. 2. (a) Daily rainfall time series from 1 Jun to 30 Sep 1968 averaged over the grid points from 12.5° to 15°N and from 10°W to 10°E (bars). Values are expressed in mm. The black area behind the daily rainfall values represents

computed as the seasonal-filtered signal where only rainfall fluctuations greater than 60 days are retained by using a nonrecursive filter (Scavuzzo et al. 1998). These computations (in Fig. 2 as well as in Fig. 3) have been done of the time series from 1 March to 30 November to avoid edge effects. The domain 10°W–10°E, also delineated in Fig. 1, is located in the heart of West Africa and in Fig. 2a it captures the different rainfall sequences described in Fig. 1. The rainfall seasonal cycle over this area is very clear with weaker rainfall at the beginning and at the end of the time series, and with the greatest values in August when the ITCZ is located at its northernmost latitude. Sequences longer than 10 days of persistent high or low rainfall amounts can also be noticed along the course of the monsoon season, consistent with Fig. 1. The wavelet diagram of the rainfall time series (Fig. 2b) highlights this intraseasonal timescale variability as intermittent signals with more variance into two-period intervals, the first between 10 and 25 days and the second between 25 and 60 days. The signal in the 25–60-day band is related to the three low rainfall sequences occurring, first before the monsoon onset in the second half of June, second at the beginning of August, third in mid-September; and to the two high rainfall sequences, in mid-July and in the second half of August. The signal in the 10–25-day band represents shorter time fluctuations occurring at different stages of the monsoon season. The Fast Fourier Transform (FFT) spectrum computed over the whole June–September period is shown in Fig. 2c. Intraseasonal variability appears clearly in the band of 40 days and in the band between 15 and 20 days. The range of the variance in these spectral bands is of the same order as the range for the seasonal signal. Figures 2d–f show similar diagrams but for a rainfall time series averaged over a more local domain 12.5°–15°N, 2.5°W–2.5°E. In this case, short time variability is enhanced, due to the local scale influence of MCS and of synoptic-scale easterly waves. However, even at this smaller spatial scale, rainfall variability due to intraseasonal-scale fluctuations is still maintained at a high level of variance (Fig. 2e). The FFT spectrum (Fig. 2f) shows a weaker variance for the seasonal cycle, enhanced variance at the two intraseasonal-scale bands, and a higher signal for periodicities lower than 5 days. Significance tests have been applied on the FFT spectra by following the procedure similar to the one used in Burpee (1972) and Diedhiou et al. (1998). One thousand series of 122 elements have been randomly generated and FFT has been performed on each series. For each harmonic, the threshold of the upper 5% of total variance fraction has been selected among the 1000 values. It represents between 4% and 5% of the variance for each harmonic. For the two FFT spectra of Fig. 2, the seasonal peak, the 40 peak and the 15–20 peak are all significant peaks. They are equal to 18.0%, 16.7%, 8.7%, respectively, for the spectrum of the regional rainfall index (Fig. 2c), and 4.8%, 9.6%, 6.4%, respectively, for the spectrum of the local rainfall index (Fig. 2f).

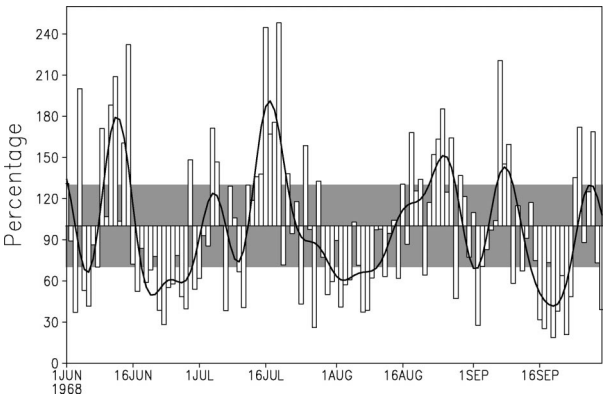

FIG. 3. Daily rainfall time series from 1 Jun to 30 Sep 1968, averaged over the domain 12.5°–15°N, 10°W–10°E. Bars represent the ratio of the unfiltered rainfall to the seasonal-filtered rainfall signal where only periodicities greater than 60 days are retained. The black curve represents the similar ratio but is filtered to remove periodicities lower than 10 days. These values are expressed in percentages of the seasonal timescale signal. The gray area is bounded by the levels of 130% and 70%.

To better characterize the intraseasonal timescale rainfall fluctuations and to clearly separate them from interannual variability, we used the following procedure. First we define a seasonal cycle specific to each year by computing the low-filtered rainfall time series where only periodicities greater than 60 days are retained. Figures 2a and 2d show such seasonal cycles (the black curve) determined for 1968. Then for each day of this year we compute the ratio of the daily rainfall to the seasonal cycle. We then obtain a daily rainfall anomaly related to the seasonal cycle of this year. It enables the removal of the effect of interannual variability that would have been present if we computed a mean seasonal cycle by averaging each daily value over the period 1968–90 for instance. Figure 3 shows the corresponding time series for 1968, averaged over the domain 12.5°–15°N, 10°W–10°E (bars). The black curve represents the similar ratio but filtered to remove periodicities lower than 10 days (due to easterly waves and

←

the daily values of the seasonal rainfall cycle computed as the seasonal-filtered signal where rainfall fluctuations lower than 60 days are removed. (b) Modulus of the wavelet analysis of the daily rainfall time series presented in (a). Only periods lower than 120 days are presented. Horizontal lines delineate periods of 10, 25, and 60 days. Values greater than 1 are shaded. (c) FFT spectrum of the daily rainfall time series presented in (a). (d) Same as (a) but for the daily rainfall time series averaged from 12.5° to 15°N and from 2.5°W to 2.5°E. (e) Same as (b) but for the daily rainfall time series presented in (d). (f) Same as (c) but for the daily rainfall time series presented in (d).

MCS activity) and to focus on intraseasonal variability. These values are expressed in percentages of the seasonal timescale signal. For instance, a value of 120% for one day on the black curve means that the rainfall modulation due to the 10–60-day variability represents a positive fluctuation of 20% of the rainfall modulation due to the seasonal cycle for this day. The different intraseasonal rainfall sequences, already shown in the previous figures, are highlighted in Fig. 3. Some of them last more than 10 days with a maximum departure level greater in absolute value than 30% of the rainfall amount due to the seasonal cycle. This represents high modulations of the rainfall regime over West Africa during northern summer and contributes significantly to the total rainfall amount of the monsoon season. It also suggests that there must be a persistent effect in temporal rainfall fluctuations at timescales higher than those due to the synoptic easterly waves or to the MCS.

From this analysis performed on the summer 1968, it appears that intraseasonal timescale variability, characterizing rainfall fluctuations in the 10–60-day range, can be a significant timescale in the West African monsoon dynamics, not only when considering rainfall averaged on a regional area but also at a local scale. This topic is now explored on the period 1968–90 and with other atmospheric variables, by performing composite analyses based on the regional rainfall index computed on the domain 12.5°–15°N, 10°W–10°E for the summers of the period 1968–90.

4. Composite intraseasonal sequences of the regional rainfall index

The black curve in Fig. 3 represents the ratio of the 10–60-day filtered rainfall to the seasonal cycle value for each day of the summer of 1968 expressed in percentages of the seasonal timescale signal. For instance, a value of 120% for one day on the black curve means that the rainfall modulation due to the 10–60-day variability represents a positive fluctuation of 20% of the rainfall modulation due to the seasonal cycle for this day. Figure 4 shows the histogram of these ratios gathering all 122 days of the 23 summer time series from 1968 to 1990 (bars). Black full line shows the same computation but for the 10–25-day filtered signal instead of the 10–60-day signal, and the dashed–dotted line is for the 25–60-day filtered signal. We chose a separation at 25 days because the wavelet diagrams are similar to the ones in Fig. 2b but, for the other years, indicate that such a separation of the spectral interval of 10–60 days is reasonable since there is always a minimum of variance around this periodicity (not shown). In Fig. 4, the distributions for the 10–60- (bars), 10–25- (full line), and 25–60-day (dashed–dotted line) values are rather symmetric with maxima centered on 100% of the seasonal cycle (that is a null contribution of the intraseasonal-scale rainfall fluctuations). However these distributions extend away from this centered value

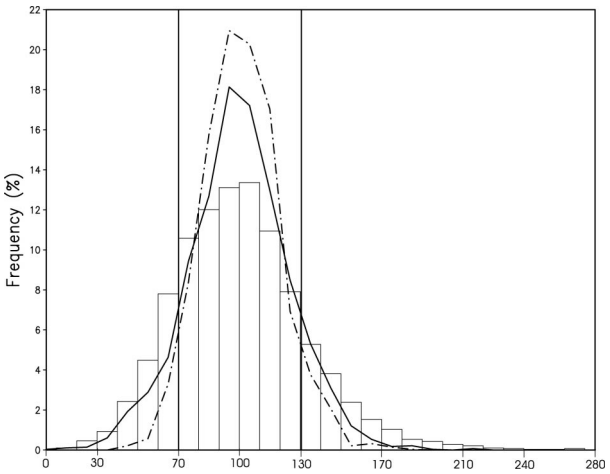

FIG. 4. Histogram of the ratio of the daily regional rainfall index (after filtering periodicities lower than 10 days) to the seasonal-filtered daily rainfall signal (where only periodicities greater than 60 days are retained). This histogram gathers all the days of the 23 summer time series from 1968 to 1990 (bars). The black full line shows the same computation for the ratio of the 10–25-day filtered signal to the seasonal-filtered signal, and the dashed–dotted line shows the ratio of the 25–60-day filtered signal to the seasonal-filtered signal. Vertical lines represents the levels 70% and 130%.

and we get a high amount of intraseasonal-scale daily rainfall fluctuation occurrences greater than 30% in absolute value: 15.8% greater than 130% and 16.3% lower than 70%. These occurrences of extreme values are the most frequent for the 10–60-day filtered signal, then for the 10–25-day filtered signal, and finally for the 25–60-day filtered signal, but the differences are small. This result means that the existence of an intraseasonal timescale modulation of daily rainfall like the one observed during the summer monsoon in 1968 is valid for the whole period 1968–90.

To better characterize these intraseasonal timescale modulations of daily rainfall over West Africa, composite analyses have been performed on all 23 summers. For each summer, we retained the dates (called t_0) where the regional rainfall ratio, similar to the one represented by the full line in Fig. 3, is maximum (minimum) and greater (lower) than 130% (70%) to define wet (dry) sequences. These rainfall modulations represent the contribution of the 10–60-day variability to the seasonal cycle. As said before, a value of 120% means that the rainfall modulation due to the 10–60-day variability represents a positive fluctuation of 20% of the rainfall modulation due to the seasonal cycle. We computed the corresponding mean composite time sequences, from $t_0 - 10$ days to $t_0 + 10$ days, by averaging all the wet sequences and all the dry sequences, using t_0 as the time reference (bars in Fig. 5a). Over the period 1968–90 we got an average of 3.9 wet and 4.5 dry sequences per season during June–September, with the highest occurrences in June (30%) and the lowest ones in August (18%). The mean modulation of the regional rainfall amount is quite high, up to 160% for wet sequences and

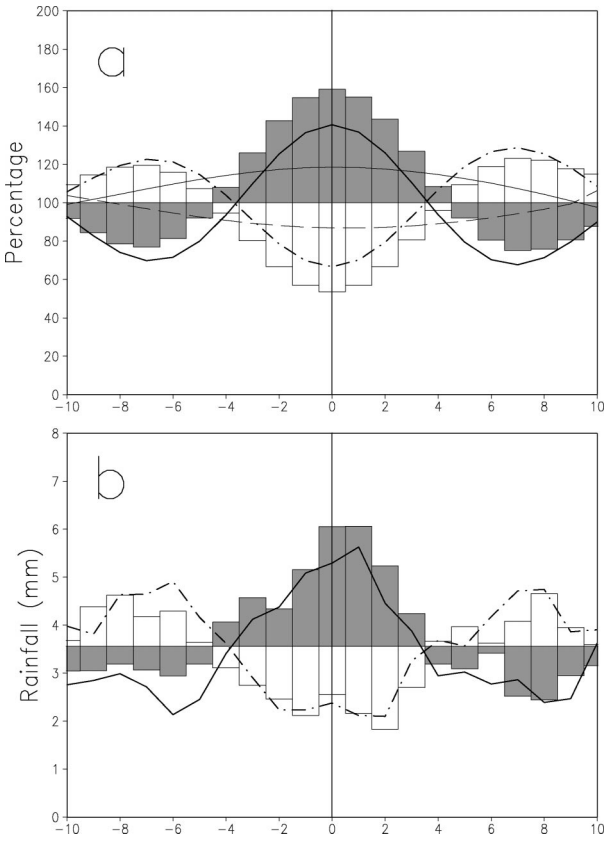

FIG. 5. (a) Time series of wet (black bars) and dry (white bars) mean composite time sequences of rainfall modulation averaged over the domain 12.5°–15°N, 10°W–10°E. These values represent the ratio of the daily rainfall, where periodicities lower than 10 days are removed, to the seasonal-filtered rainfall signal where only periodicities greater than 60 days are retained. They are expressed in percentages of the seasonal timescale signal. The wet (dry) composites have been computed by selecting days over the periods Jun–Sep 1968–90 where the regional rainfall ratio is a max (min) and is greater than 130% (lower than 70%) of the seasonal timescale signal. All these wet (dry) sequences have been averaged by considering as the reference data t_0 the days of max (min) percentage and by computing the averages of the percentages from $t_0 - 10$ days to $t_0 + 10$ days. The full (dashed–dotted) curve shows the composite wet (dry) sequence determined from the same t_0 reference dates but by averaging values from the 10–25-day filtered signal. The thin full (dashed) curve shows the composite wet (dry) sequence determined from the dates t_0 reference dates but by averaging values from the 25–60-day filtered signal. (b) (bars) Same as (a) but for the composite sequences computed with the same t_0 reference dates by using the regional rainfall values without dividing by the seasonal-filtered signal. The full and dashed-dotted curves represent sequences similar to the ones displayed with bars but from the t_0 reference dates determined from the 10–25-day filtered regional rainfall signal.

down to 60% for dry sequences. These sequences are preceded and followed by weaker rainfall anomalies of the opposite sign. Whereas the signal results from the rainfall variability between 10 and 60 days, the mean wet and dry sequences last 9 days and belong to a quasi-periodic fluctuation whose corresponding period is quite short, about 15 days. Similar computations done from the same t_0 reference dates but with the 10–25-day filtered signal (full and dashed–dotted curves in Fig. 5a) confirm this conclusion by showing quite similar time sequences with only small differences: the 10–25-day mean composite sequences have a similar periodicity and consist of more symmetric fluctuations with weaker rainfall anomalies around t_0 and higher anomalies of opposite signs ($t_0 - 7$ and $t_0 + 7$). These differences are due to the influence of the 25–60-day variability. Computations done with this signal led to a composite periodicity at about 38 days with rather weak rainfall fluctuations (see thin full and dashed curves in Fig. 5a). So the whole 10–60-day signal is dominated by the 10–25-day signal. Figure 5b shows, displayed with bars, similar composite sequences computed with the same t_0 reference dates but using the regional rainfall values without dividing by the seasonal-filtered signal. We see that at t_0 the difference of the mean rainfall amount between the mean wet and dry phases is very high, from 2 to 6 mm day^{-1}, confirming the significance of an intraseasonal timescale variability in the monsoon dynamics over West Africa. The full and dashed–dotted curves represent sequences similar to the ones displayed with bars but from the t_0 reference dates determined from the 10–25-day filtered regional rainfall signal. It provides highly similar sequences, confirming the dominance of the 10–25-day variability on intraseasonal timescale rainfall fluctuations.

Similar computations have been performed on OLR values averaged on the same domain 12.5°–15°N, 10°W–10°E over the period 1979–90. Due to the scale value of this variable (values between 210 and 240 W m^{-2} in the ITCZ), the threshold levels selected are 95% and 105% of the seasonal-filtered signal. The results obtained are quite consistent with those from the rainfall values, with high variations between wet and dry sequences, up to 40 W m^{-2}, from 220 from the wet sequence at t_0 to 260 W m^{-2} for the dry sequence at t_0 (not shown).

We have confirmed in this section that rainfall variability at intraseasonal timescale is a significant feature of the West African monsoon, and that it is mainly defined by fluctuations between 10 and 60 days, with a dominant periodicity range between 10 and 25 days. So, in the following, we focus on the intraseasonal timescale fluctuations between 10 and 25 days, and look at the connections between this rainfall regime and atmospheric circulation.

5. Composite intraseasonal sequences of enhanced/weakened monsoon phases

a. Mean convection and wind fields at t_0

Unfiltered mean convection and wind fields have been computed for the composite 1968–90 summer wet and dry sequences at t_0, the different t_0 times for the wet (dry) sequences being selected when the 10–25-day filtered regional rainfall index is maximum (min-

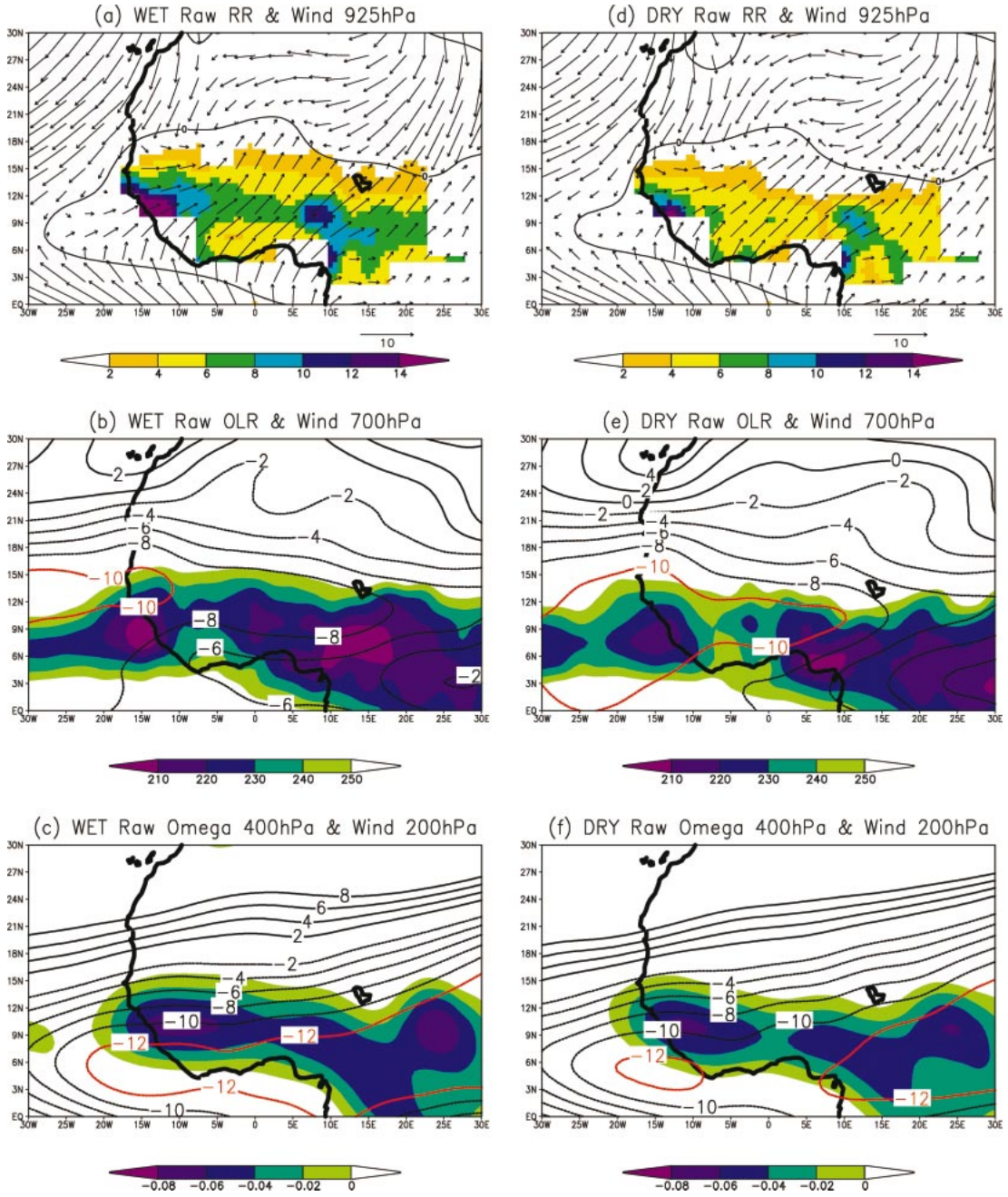

FIG. 6. (a) Unfiltered mean rainfall and 925-hPa wind fields for the composite 1968–90 summer wet sequence at t_0. Rainfall is displayed in colors and expressed in mm day^{-1}. The wind is expressed in vectors and its scale (m s^{-1}) is displayed below. The black line represents the zero isoline of the zonal wind component to delineate the domain of the monsoon wind. (b) Same as (a) but for the OLR values (colors, in W m^{-2}) and the wind speed at 700 hPa (isolines in m s^{-1}). (c) Same as (a) but for the NCEP–NCAR vertical velocity at 400 hPa (colors, Pa s^{-1}) and the wind speed at 200 hPa (isolines in m s^{-1}). (d) Same as (a) but for the composite dry sequence at t_0. (e) Same as (b) but for the composite dry sequence at t_0. (f) Same as (c) but for the composite dry sequence at t_0. Wet (dry) sequences are selected when the 10–25-day filtered regional rainfall index is max (min) and greater (lower) than 30% of the seasonal-filtered rainfall signal.

imum) and greater (lower) than 30% of the seasonal-filtered rainfall signal. Figure 6a shows the corresponding rainfall and 925-hPa wind fields for the wet sequence at t_0. The black line represents the zero isoline of the zonal wind component to delineate the domain of the monsoon winds. Figure 6d shows the similar fields for the dry sequence. The impact of the 10–25-day intraseasonal variability on the ITCZ rainfall field appears in these two figures as very high through the differences in the rainfall amounts and their spatial

extent, which confirms the previous results. We observe very clearly that during a dry phase, rainfall over West Africa is lower that during a wet phase, convection is strongly decreased in the heart of the ITCZ, and the northern boundary of the rainfall area is displaced by several degrees to the south. The amplitude of the rainfall difference is very high related to its mean as seen in Fig. 5b. Moreover, the rainfall modulation between a wet phase and a dry one concerns the whole of West Africa, both in latitude and in longitude, meaning that these intraseasonal timescale variations belong to an extended spatial pattern. During a dry phase, the northern boundary between the dry northeasterly winds and the moist southwesterly winds, delineated by the zero isoline of the zonal wind component, is weakly modified except a southward displacement at the longitude of Lake Chad (15°E). We also observe that the area of the southwesterly winds over the tropical Atlantic off the western coast of West Africa is less extended, meaning a weaker moisture advection over West Africa.

Figures 6b and 6e show similar fields for OLR and the wind speed at 700 hPa. OLR values are consistent with rainfall values, highlighting the deep convection decrease in the ITCZ during a dry phase. The wind fields characterize the location of the African easterly jet (AEJ) in the midlevels of the troposphere, and show an increase of the speed of this jet during a dry phase by about 2 m s^{-1}. At higher levels (Figs. 6c and 6f), the NCEP–NCAR upward velocities at 400 hPa are also weaker in the ITCZ during a dry phase, and the wind speed at 200 hPa, describing the tropical easterly jet (TEJ), is also weaker by about 1 m s^{-1}. It is worth noticing that the differences in the dynamical features of the West African monsoon between wet and dry phases at the intraseasonal timescale are similar to the ones observed at the interannual timescale (Newell and Kidson 1984; Fontaine and Janicot 1992). We suggest that similar connections between convection and the atmospheric circulation over West Africa must operate at both these timescales.

b. *Time sequence of convection and low-level wind fields*

Figure 7 shows the composite ''wet–dry'' time sequence of the unfiltered rainfall and 925-hPa wind fields from $t_0 - 7$ days to $t_0 + 7$ days by a step of 2 days. As for Fig. 6, wet (dry) sequences are selected when the 10–25-day filtered regional rainfall index is maximum (minimum) and greater (lower) than 30% of the seasonal-filtered rainfall signal. The rainfall values displayed in the figure are the ratio of the wet–dry-unfiltered rainfall to the seasonal-filtered rainfall signal. They are expressed in percentages of the seasonal timescale signal.[1] The corresponding composite 925-hPa wind field is computed as the unfiltered wind difference between the wet and the dry sequences. All the unfiltered fields presented in Fig. 7 and in the following figures are very similar to the filtered ones computed from the 10–25- or the 10–60-day filtered values. As the rainfall fields have a limited geographical extension, due to the limited available dataset, Fig. 8 shows the same sequence but on a larger domain by using OLR values. In this figure, the wind fields, displayed by streamlines, have been computed using a 3-day moving average to get a bit smoother fields for a better clarity; OLR values are the unfiltered wet–dry differences, not expressed in percentages as it is done for rainfall. Rainfall fields in Fig. 7 (computed from the period 1968–90) and OLR fields in Fig. 8 (computed from the available period 1979–90) show very similar anomalies, and both are very consistent with the wind anomaly fields (computed from the period 1968–90 in both Figs. 7 and 8). It is worth while to repeat that all these datasets come from independent measurements. The vector fields in Fig. 7 provide the amplitude of the wind anomalies and the streamlines in Fig. 8 help to better see the patterns of the wind fields.

Patterns in Figs. 7 and 8 characterize the modulations due to a typical intraseasonal wet phase occurring over West Africa. Reverse patterns must be considered for a typical dry phase. The total wind fields are the superposition of these modulations on the mean wind field presented in Figs. 6a and 6d. At this stage of the study, we do not provide any mechanism to explain the onset and the development of such a typical intraseasonal wet phase. Doing so would require us to focus on individual cases. Here by the composite approach based on large datasets we only document how convection and atmospheric circulation patterns are modulated during this composite time sequence. At the end of this part, we add some comments about how this can be interpreted.

At $t_0 - 7$, rainfall deficit over West Africa is at the highest stage, preceding the following setup of the intraseasonal wet sequence; at this time the regional rainfall index for the wet sequence has its lowest value before the convective maximum (Fig. 5). This dry stage is consistent with an extended enhanced advection of dry air from a northerly low-level atmospheric circulation. This circulation is first associated with the enhancement of the anticyclonic circulation centered at 20°N, 25°W, second with the enhancement of the cyclonic center located above Lake Chad (15°N, 15°E)

[1] We first compute the mean wet rainfall anomaly expressed in percentages of the seasonal timescale signal, averaged for all the wet retained cases. For instance, a value of 120% means that the rainfall modulation due to the wet cases represents a mean positive fluctuation of +20% of the rainfall modulation due to the seasonal cycle. We do the same for the dry cases, say for instance 70%, that is a modulation of −30%. We compute the wet minus dry difference, that is (+20) − (−30) = +50% and we express this value as 150% in Fig. 7.

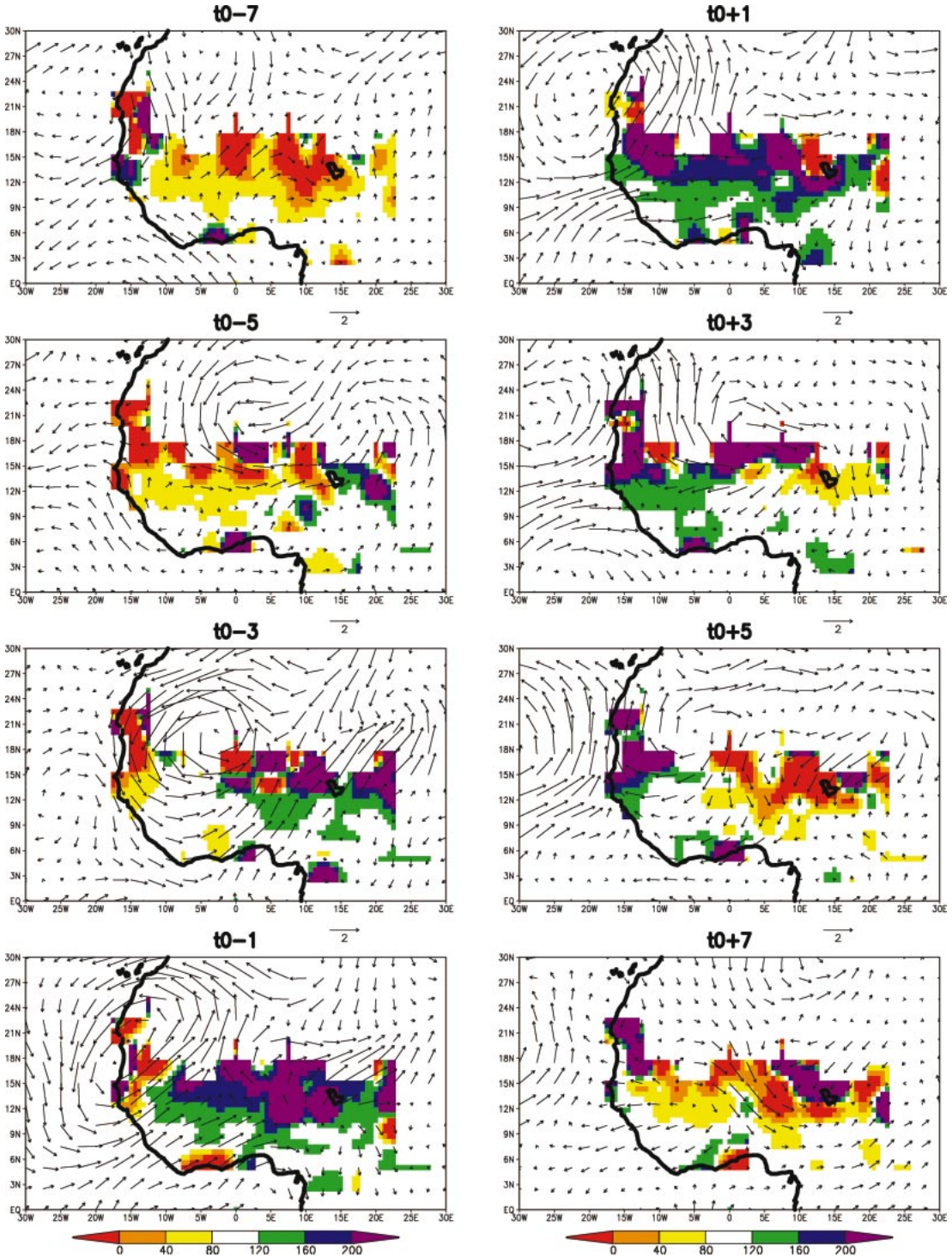

FIG. 7. The composite 1968–90 wet–dry time sequence of the unfiltered rainfall field (colors) and the 925-hPa wind field (vector) from $t_0 - 7$ days to $t_0 + 7$ days by a step of 2 days. Wet (dry) sequences are selected when the 10–25-day filtered regional rainfall index is max (min) and greater (less) than 30% of the seasonal-filtered rainfall signal. The rainfall values displayed in the figure are the ratio of the daily unfiltered rainfall to the seasonal-filtered rainfall signal. They are expressed in percentages of the seasonal timescale signal and displayed for values lower than 80% and greater than 120%. The corresponding composite 925-hPa wind field is computed as the unfiltered wind difference between the wet and the dry sequences. The scale (m s^{-1}) is displayed below.

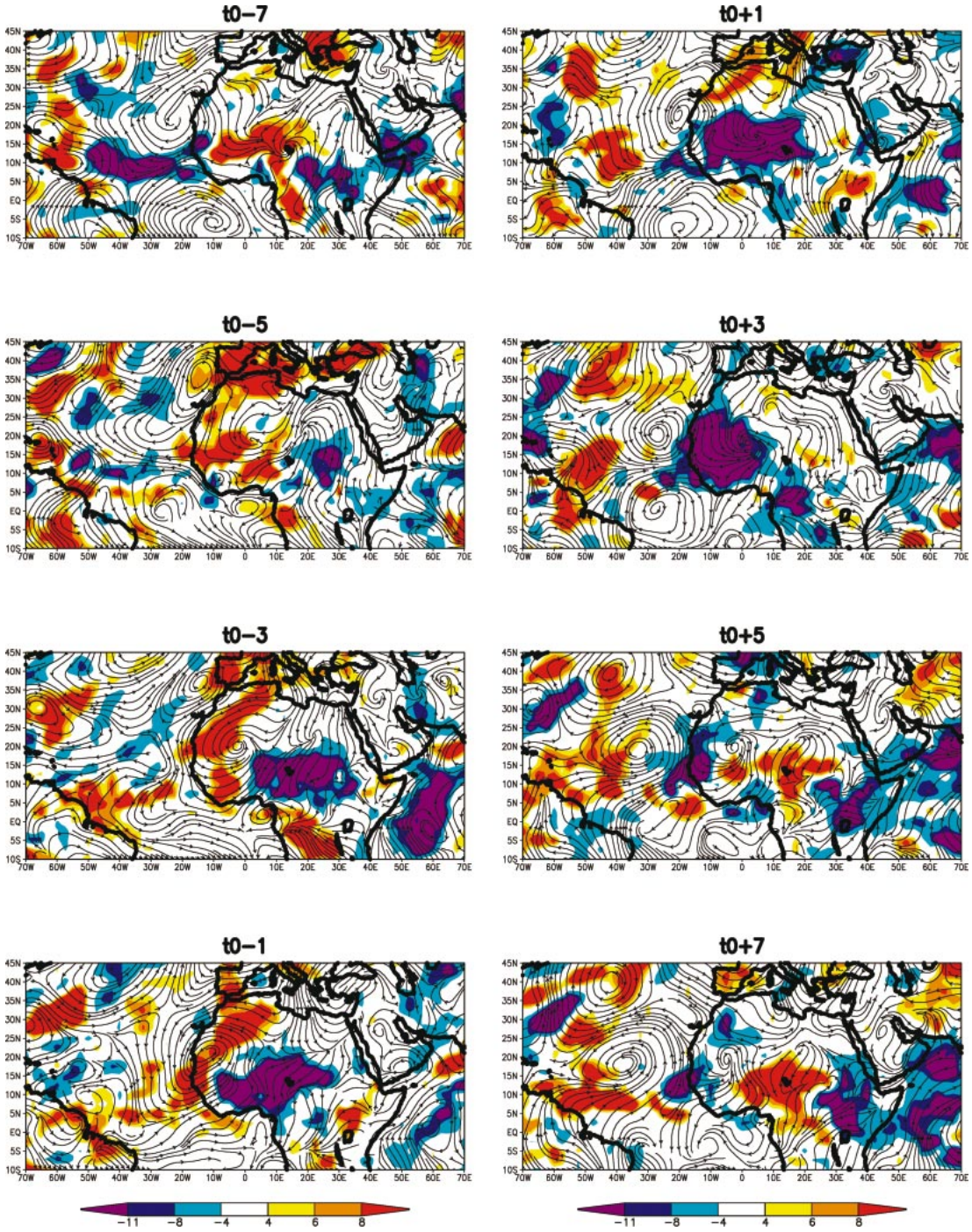

FIG. 8. Same as Fig. 7 but for OLR values instead of rainfall values, and displayed on a wider domain. In this figure, the 925-hPa wind fields are displayed by streamlines and have been computed using a 3-day moving average to get a bit smoother field for better clarity. The composite OLR sequence has been computed from the available period 1979–90 and the composite wind sequence from the period 1968–90. OLR values (W m^{-2}) are the unfiltered value differences between wet and dry sequences, and not expressed in percentages as it is done for rainfall on Fig. 7.

with a northeast–southwest axis of the associated trough. The area of decrease convection over West Africa is surrounded westward and eastward by enhanced convective areas that represent the preceding (westward) and the coming (eastward) intraseasonal wet phases (Fig. 8).

At $t_0 - 5$, positive rainfall anomalies associated with the coming wet phase appear in the northeastern part of

the domain. Figure 8 shows that this enhanced convective area first developed over central Africa in an increased southerly wind field linked to the enhanced trough located along 20°E over the Sahara. At this time, two abnormal cyclonic centers are present, the first one at 20°N, 0°, already seen above Lake Chad at $t_0 - 7$, which has moved westward, the second one being stationary at 20°N, 15°E. These two cyclonic centers are associated with an increased westerly wind field over most of West Africa.

At $t_0 - 3$, the enhanced convective area is now well developed east of 0° in the enhanced southwesterly wind field associated with the two cyclonic centers, the first one continuing westward and now centered at 20°N, 5°W, whereas the second one is still stationary at 20°N, 20°E. These two centers, separated by about 25° longitude, lead to a zonally extended area of enhanced moist southwesterly winds over West Africa, consistent with the buildup of a similarly extended area of enhanced convection in the ITCZ.

At $t_0 - 1$, the first cyclonic center is now located along the western coast of West Africa and the enhanced convective area extends westward in the increased southerly winds located east of this center, covering most of West Africa. The second cyclonic center remains between 20° and 30°E, and is linked, with the first center, to the enhanced southwesterly wind field over all of West Africa. In the southwesterly wind field between the two cyclonic centers, an abnormal anticyclonic ridge appears northwest of Lake Chad. This indicates the following cutoff of the large cyclonic circulation over West Africa, due to the fact that the first cyclonic center continues on westward whereas the second one is still maintained around 20°E. We notice at this stage that the positive anomalies of rainfall and convection cover the whole area where the ITCZ is located during northern summer, with the highest values located on the northern boundary of the ITCZ, that is, the latitudes of the Sahel area where we find most of the MCS trajectories. This is consistent with the rainfall and OLR patterns of Fig. 6 where we observe both the enhanced convection in the ITCZ and the northward extension of its northern boundary during a wet phase.

At $t_0 + 1$, all of West Africa in under the influence of the wet intraseasonal phase despite the fact that the ridge has now developed into a closed anticyclonic circulation at 15°N, 5°W. This may be due to the convergence between abnormal southwesterly winds still associated with the first cyclonic center now located at 20°W and abnormal easterly winds along 10°N associated with the anticyclonic center. A second abnormal anticyclonic circulation is now formed above Lake Chad (it was slightly formed at $t_0 - 1$) and is linked to an abnormal northerly wind field over central Africa, that is, weakened southerly winds. This wind field has merged with the enhanced northerly wind field located above the Sahara previously associated with the second quasi-stationary cyclonic center, which leads then to a large abnormal northerly wind field evident from 45°N to 10°S along 20°E. These dry northerly winds also mark very clearly the eastern boundary of the enhanced convection area of the wet phase. It is worth noting at this stage the evidence of another abnormal cyclonic circulation centered at 40°N, associated with the increased northerly winds at 20°E and north of 20°N since $t_0 - 3$. The role of atmospheric interactions from midlatitudes in the initiation of these intraseasonal timescale sequences over West Africa should be considered, but it is out of the scope of this paper.

At $t_0 + 3$, the enhanced convective area is now located westward of 0° in the remaining enhanced southerly winds located between the cyclonic center at 30°W and the anticyclonic center at 0°. The enhanced convective area may have been also maintained since $t_0 - 1$ by a stronger westerly moisture advection located over the tropical Atlantic off the western coast of West Africa. Behind the anticyclonic center, enhanced northerly winds develop and are associated with the extension of the dry phase following the wet phase. Negative values for rainfall and positive values for OLR appear east of Lake Chad, in concomitance with the increased northerly winds previously present at 20°N and now associated with a new anticyclonic ridge north of 20°N and between 10° and 30°E.

At $t_0 + 5$, the positive rainfall and negative OLR anomalies associated with the wet phase are now limited along the western coast of West Africa while the cyclonic center goes on propagating westward over the tropical Atlantic. We note a northward extension of these anomalies along the coast up to North Africa, already present in the preceding days, in the latitudinaly extended area of abnormal southerly winds. The weakened convective area is now widely developed east of 0° in the abnormal northerly winds now covering most of West Africa and are both associated with the westward-moving anticyclonic center and the development of the anticyclonic ridge at 20°E. East of this decreased convective area, a new enhanced convective area is developing above eastern-central Africa in increased southerly winds, which will become the next intraseasonal wet phase.

Finally, at $t_0 + 7$, the weakened convective area goes on propagating westward. This stage corresponds to the time where the regional rainfall index for the wet sequence has its lowest value after the convective maximum (Fig. 5). This area is surrounded westward and eastward by enhanced convective areas that first represent (westward), the preceding wet phase associated with the cyclonic center still moving westward over the tropical Atlantic, and second (eastward), the next developing wet phase.

In this description, we have not attempted to introduce any cause and effect relationship. Instead, at this stage we introduce the concept of the ''suprasynoptic'' scale developed for the medium-range forecast (Persson 1984; Atger 2000). The idea is that the range of predictability

depends on the spatial scale of the phenomena that we want to predict. So to achieve reliable medium-range forecasts beyond 3 days, we must give up the synoptic scale and consider a larger scale, the suprasynoptic scale where the synoptic details are smoothed or filtered. Such suprasynoptic patterns appear to be similar to the classic synoptic fields except that they belong to a larger spatial scale and that they develop and propagate more slowly. This can be associated with the concept of weather types that induce specific characteristics and distributions of the classic synoptic weather systems. This is what we observe over West Africa (Fig. 8) where the wind field patterns are similar to the synoptic-scale easterly waves but with a greater wavelength (about 6000 km for the suprasynoptic scale instead of 3000 km for the synoptic scale) and a slower westward propagation (4° lon day^{-1} instead of 8° day^{-1}), finally giving a period of about 15 days for the suprasynoptic scale instead of 4 days for the synoptic scale. We do not provide any mechanism for the occurrence of such weather types but we show their existence and indicate that they represent a modulation of the synoptic-scale activity at a larger scale. This corresponds to the dominant periodicities that we highlighted at the 10–25-day range, and not necessarily to the longer timescale, 25–60-day, which may be more specific to the intraseasonal timescale such as for the Madden–Julian Oscillation (MJO) for instance (Matthews 2002).

We can consider more precisely the modulation of the synoptic-scale easterly wave activity by the intraseasonal variability. Easterly wave activity over the Sahel can be characterized by the 700-hPa meridional wind component at 15°N, 0° (Diedhiou et al. 1999). Figure 9 displays the mean 1968–90 intraseasonal wet–dry composite of the wavelet modulus of the NCEP–NCAR 700-hPa meridional wind component at 15°N, 0°, from $t_0 - 15$ to $t_0 + 15$. Wavelet analyses have been completed separately for each wet and dry time sequence. Then, the individual ''wet'' wavelet spectra have been averaged, as well as the individual ''dry'' wavelet spectra, and we finally computed the difference of the two mean spectra. Figure 9a shows an enhancement of the easterly wave fluctuations for the periodicities 2.5–8 days from $t_0 - 2$ and $t_0 + 4$ during a typical intraseasonal wet sequence. It represents about 20% of the mean signal associated to these waves. When integrating the values of this diagram over the periods 2.5–10 days, we can observe a mean periodicity of 14 days for the amplitude of the wavelet signal, with a maximum at $t_0 + 1$ and two minima at $t_0 - 6$ and $t_0 + 8$ (Fig. 9b). Such variability in the easterly wave activity over the Sahel has recently been pointed out for the individual year 1992 (Redelsperger et al. 2002). We show here that it is valid for a high number of years and that it is embedded in a specific mode of intraseasonal variability that we designed as suprasynoptic.

As it was noticed previously, the distribution of the wet and the dry phases is not strictly uniform along the

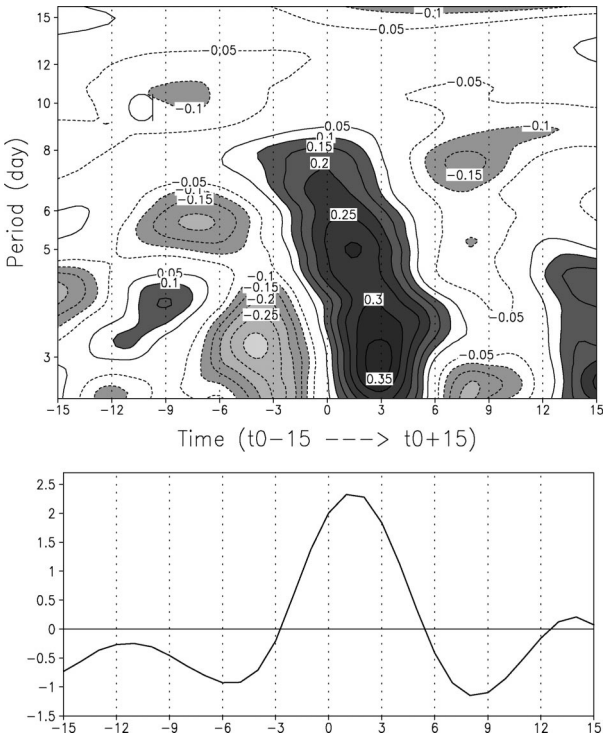

FIG. 9. Mean 1968–90 intraseasonal wet–dry composite of the wavelet modulus of the NCEP–NCAR 700-hPa meridional wind component (m s^{-1}) at 0°, 15°N, from t_0 minus 15 days to t_0 plus 15 days. (a) Only periods lower than 15 days are presented. Values greater than 0.1 are shaded. (b) The modulus time series generated by scale averaging over the 2.5–10-day period band is expressed in standardized anomalies.

northern summer. Their occurrences are the highest in June (30%) and the lowest in August (18%). An automatic classification (Janicot 1992) of the 10–25-day 925-hPa wind field patterns at t_0 has been performed for separately the wet and the dry phases into three classes. The three classes are seasonally distributed, one class gathering most of the phases of June, another class the phases for July–August, and a last one for September. Then, when recomputing the difference wet–dry fields at t_0 for the ''June'' class, the ''July–August'' class and for the ''September'' class, we get three wind field patterns close to the composite one of Fig. 7, but with a strong and well-organized July–August field, a rather well-organized September field, and a weaker organized June field (not shown). So the intraseasonal phase distribution is a bit biased toward June, but the composite summer wind fields are more representative of the July–August and the September phases, that is, in the heart of the West African summer monsoon.

Figure 10 displays the longitude–time diagram of the wet–dry sequence of unfiltered OLR along the latitude band 12.5°–15°N, from $t_0 - 25$ to $t_0 + 25$, and from 40°E to 70°W. This diagram highlights the westward propagation of longitudinally extended areas of enhanced and weakened convection already seen over

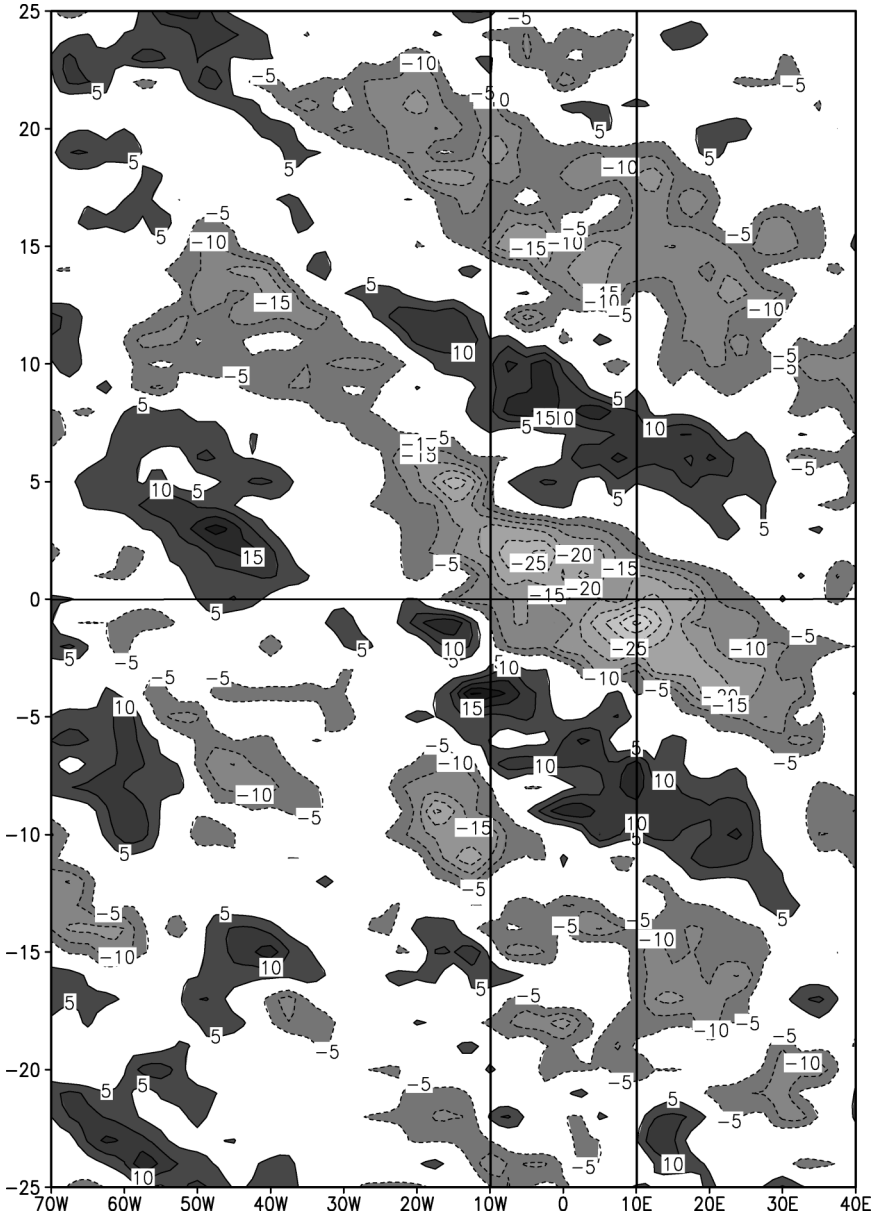

FIG. 10. Lon–time diagram of the composite 1979–90 wet–dry sequence of the unfiltered OLR values along the latitude band 12.5°–15°N, from $t_0 - 25$ days to $t_0 + 25$ days. The computation method is the same as for Fig. 8. Vertical lines delineate the area 10°W–10°E.

West Africa but that, in fact, extend from eastern Africa to the western tropical Atlantic. The signal associated to the wet–dry phase over West Africa at t_0 disappears along 50°W because the OLR anomalies move northward at $t_0 + 15$, where they are still evident on the three following days (not shown). The signal is logically the greatest over West Africa around t_0 since it has been selected through the regional rainfall index on this area, and the highest values go up to more than 30 W m^{-2} in absolute value. We also observe that the typical wet sequence centered on t_0 is embedded in a sequence of several intraseasonal phases, two of them before it and two of them after it. As these phases were computed from unfiltered values, this figure highlights the significant modulation of convection over West Africa at an intraseasonal timescale centered around 15 days, as seen in Fig. 5.

c. *Vertical structure of the intraseasonal signal*

Figure 11 shows latitude–pressure cross sections along the band 10°W–10°E of the meridional circulations associated with the intraseasonal signal. For simplicity, we use here the ''Hadley'' nomenclature whereas

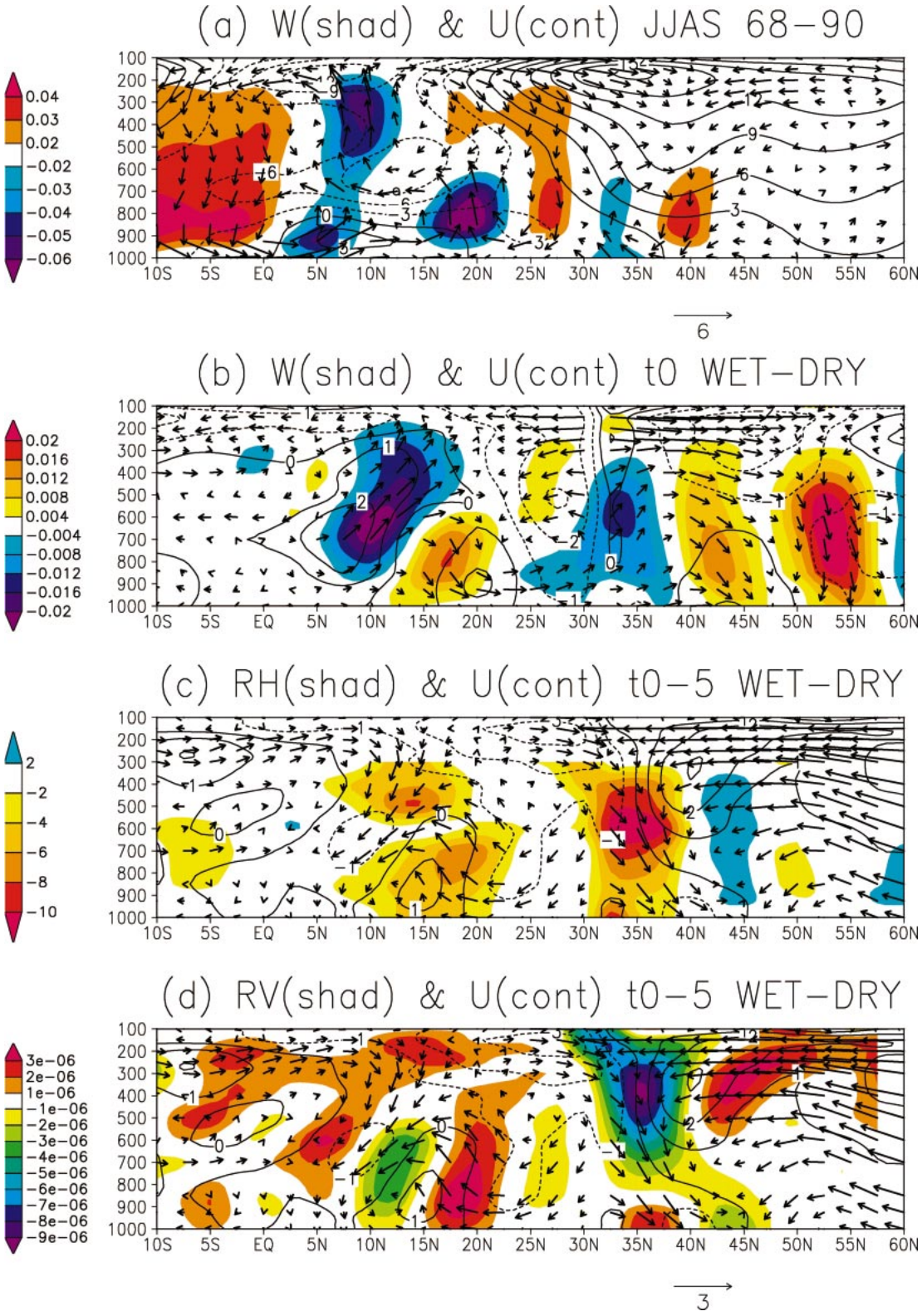

FIG. 11. (a) Lat–pressure cross section of the (10°W–10°E) averaged meridional circulation computed on Jun–Sep 1968–90. Vectors display the (v, w) circulation, colors the amplitude of the vertical velocity (negative upward), and isolines the zonal wind (m s^{-1}). (b) Same as (a) but for the unfiltered mean meridional-vertical wind field of the composite 1968–90 summer wet–dry sequence at t_0. The vertical velocity is displayed in colors and expressed in Pa s^{-1}. The zonal wind component is displayed in isolines (m s^{-1}). (c) Same as (b) but at $t_0 - 5$ with colors representing relative humidity (%). (d) Same as (c) but with colors representing relative vorticity (s^{-1}).

the 10°W–10°E band is too small a longitude band to use it. Figure 11a presents the mean meridional circulation (vectors, with colors areas for vertical velocity) computed on June–September 1968–90, as well as the zonal wind component (isolines). The main features of the circulation over these regions are evident: two Hadley-type circulations with the specific structure over West Africa of upward velocities in the whole troposphere at the location of the ITCZ at 10°N, and subsiding velocities south of the equator and between 25° and 40°N; upward velocities limited to the lower troposphere associated to the dry convection in the heat low at 20°N; the westerly winds of the monsoon layer between the equator and 20°N; the two easterly jets, the AEJ in the midlevels between 10° and 15°N and the TEJ in the upper troposphere at 5°N; the subtropical westerly jet in the upper troposphere at 35°N.

Figure 11b shows the unfiltered mean meridional circulation of the composite 1968–90 summer wet–dry sequence at t_0. The vertical velocity differences are displayed in colors and the zonal wind anomalies in isolines. We see again that the specific wet phase is characterized by a stronger deep convection in the ITCZ that extends to the north, as well as a decreased dry convection in the heat low. This leads to an enhanced southern Hadley-type circulation and a weakened northern Hadley-type circulation. In consistency with the pattern of the anomalous meridional circulation, we observe positive zonal wind anomalies over West Africa depicting the enhancement of the monsoon winds in the low levels and the decrease of the AEJ in the midlevels, as well as negative anomalies in the upper levels leading to an enhancement of the TEJ and a weakening of the subtropical westerly jet. The associated relative vorticity anomaly pattern (not shown) indicates that the circulation pattern seen at 925 hPa (Fig. 7) is in fact present in the part of the troposphere under the 500-hPa level with a rather barotropic structure.

Figures 11c and 11d show similar patterns of meridional circulation but for $t_0 - 5$. At this time (see Fig. 8), the zone of enhanced convection that will be present over West Africa at t_0 is located east of Lake Chad, embedded in an enhanced southerly low-level flow linked to the cyclonic center at 20°N, 20°E. The other cyclonic center is located at 20°N, 0°. These centers are associated over West Africa with two axes of enhanced northerly dry flow, one coming from the Mediterranean Sea along 15°E, another one located between the western coast of West Africa and the Greewich meridian. This dry wind field is associated with a weakened convection over West Africa and a dry rainfall sequence preceding the occurrence of the wet sequence coming from the east. Figure 11c depicts the modulation of the mean meridional circulations on 10°W–10°E as well as the relative humidity anomalies. This circulation pattern is opposite to the one related to t_0 (Fig. 11a). At $t_0 - 5$, the subsidence in the northern Hadley-type circulation between 30° and 40°N is enhanced, linked to an abnormal wind convergence above 300 hPa, and the subsiding air is drier than normal. This air diverges at the lower levels and a part of it is directed toward the south as it has just been described (Fig. 8). Then it can mix into the heat low where dry convection increases. The zonal wind field at these levels, as well as the relative vorticity field (Fig. 11d), shows that the cyclonic vorticity increases in the heat low that extends on the vertical. This increase of the heat low activity and of the associated meridional overturning may induce a stronger intrusion of drier air into the ascending air column of the ITCZ and a weakening of deep convection and of the southern Hadley-type circulation. This abnormal mean wind field pattern may induce interactions between the midlatitudes and the ITCZ, in particular by favoring southerly advection of dry air from the northern midlatitudes as it is shown for instance in Roca et al. (2002). However this hypothesis needs a specific examination of ensembles of air parcel trajectories, which is out of the scope of this study.

6. Conclusions

Rainfall variability over West Africa has usually been analyzed either through the MCS scale, the synoptic scale, or the interannual and decadal scales. Very few studies have investigated the West African monsoon through the intraseasonal timescale. A documentation of such variability has been produced by using daily gridded datasets of rainfall, convection, and reanalyzed atmospheric fields over the period 1968–90. Rainfall and convection over West Africa are significantly modulated at two intraseasonal timescales, 10–25 and 25–60 days, leading to variations of more than 30% of the seasonal signal. A composite analysis based on the dates of maximum (minimum) of a regional rainfall index in wet (dry) sequences shows that these sequences last in average 9 days and belong to a main quasi-periodic signal of about 15 days. A secondary periodicity of 38 days is present but leads to a weaker modulation. During a wet (dry) sequence, convection in the ITCZ is enhanced (weakened) and its northern boundary moves to the north (south), while the speed of the African easterly jet decreases (increases), the speed of the tropical easterly jet increases (decreases), and the monsoon flow becomes stronger (weaker), all these features being similar to the ones associated with interannual variability characterizing wet and dry years.

This modulation of convection at intraseasonal timescales is not limited to West Africa, but corresponds to a westward-propagating signal from the eastern Africa to the western tropical Atlantic. The enhanced (weakened) phases of the West African monsoon are associated with a stronger cyclonic (anticyclonic) activity over the Sahel, linked to stronger (weaker) moisture advection over West Africa. Five days before the full development of the wet phase, a stronger cyclonic circulation at 20°E induces enhanced southerly winds along 25°E

where convection enhances, while another westward-propagating cyclonic circulation is located at 0°. This atmospheric pattern is linked to the enhancement of the subsiding branch of the northern Hadley cell at 35°N, of the northerly advection of drier air over West Africa, and to increased dry convection in the heat low at 20°N. It propagates westward leading to a zonally extended area of enhanced monsoon winds over West Africa consistent with the occurrence of the wet phase.

We have proposed to apply the concept of the suprasynoptic scale developed for the medium-range forecast. To achieve reliable medium-range forecasts beyond 3 days, the synoptic scale must be given up and a larger scale, the suprasynoptic scale must be considered where the synoptic details are smoothed or filtered. Such suprasynoptic patterns appear to be similar to the classic synoptic fields except that they belong to a larger spatial scale and that they develop and propagate more slowly. This can be associated with the concept of weather types that induce specific characteristics and distributions of the classic synoptic weather systems like easterly waves or of the MCS life cycle. We showed the existence of such weather types over West Africa and indicated that they represent a modulation at a larger scale of the synoptic-scale activity of easterly waves. This corresponds to the dominant periodicities that we highlighted at the 10–25-day range, and not necessarily to the longer timescale, 25–60 days, which may be more specific to the intraseasonal timescale such as for MJO for instance.

We did not provide any mechanism for the occurrence of such weather types; it should be the next step. One of the main questions that arose is the role of scale interactions between MCS and synoptic-scale weather systems like easterly waves (Redelsperger et al. 2002). Kiladis and Weikmann (1997), studying the 6–30-days fluctuations of convection over West Africa, suggested that such a signal could be induced by convection. This raises the question of the role that one MCS can play on the following convection. At a local scale, Taylor et al. (1997) suggested that a MCS can induce a moistening of the boundary layer, favorable to the development of a new MCS at the same location, as was observed during the Hydrology–Atmosphere Pilot Experiment in the Sahel (HAPEX-Sahel) field experiment in 1992 (Taylor and Lebel 1998). Could such a local inter-MCS connection work at a larger scale through interactions with the monsoon flow and/or synoptic easterly waves to build the intraseasonal-scale variability observed over West Africa? It is one of the questions that the international project of the African Monsoon Multidisciplinary Analyses (AMMA; information available online at http://medias.obs-mip.fr/amma) wishes to address.

Acknowledgments. We are thankful to NOAA–CIRES Climate Diagnostics Center (Boulder, CO) for providing the NCEP–NCAR reanalysis dataset and the interpolated OLR dataset from their Web site (http://www.cdc.noaa.gov/). We also thank the two anonymous reviewers who helped to improve this paper. This research was in part supported by the EC Environment and Climate Research Programme (Contract: EVK2-CT-1999-00022).

REFERENCES

Atger, F., 2000: The medium-range weather forecast in France (in French). *La Météorologie*, 8th Series, **30,** 61–86.

Burpee, R. W., 1972: The origin and structure of easterly waves in the lower troposphere in North Africa. *J. Atmos. Sci.,* **29,** 77–90.

Diedhiou, A., S. Janicot, A. Viltard, and P. de Felice, 1998: Evidence of two regimes of easterly wave over West Africa and the tropical Atlantic. *Geophys. Res. Lett.,* **25,** 2805–2808.

——, ——, ——, ——, and H. Laurent, 1999: Easterly wave regimes and associated convection over West Africa and the tropical Atlantic: Results from NCEP/NCAR and ECMWF reanalyses. *Climate Dyn.,* **15,** 795–822.

Duvel, J. P., 1989: Convection over tropical Africa and the Atlantic Ocean during northern summer. Part I: Interannual and diurnal variations. *Mon. Wea. Rev.,* **117,** 2782–2799.

——, 1990: Convection over tropical Africa and the Atlantic Ocean during northern summer. Part II: Modulation by easterly waves. *Mon. Wea. Rev.,* **118,** 1855–1868.

Folland, C. K., T. N. Palmer, and D. E. Parker, 1986: Sahel rainfall and worldwide sea temperature 1901–1985. *Nature,* **320,** 602–607.

Fontaine, B., and S. Janicot, 1992: Wind field coherence and its variations over West Africa. *J. Climate,* **5,** 512–524.

Gibson, J. K., P. Kalberg, S. Uppala, A. Hernandez, A. Nomura, and E. Serrano, 1997: ERA description. ECMWF Re-Analysis Project, Rep. Series 1, ECMWF, Reading, United Kingdom, 72 pp.

Grodsky, S. A., and J. A. Carton, 2001: Coupled land/atmosphere interactions in the West African monsoon. *Geophys. Res. Lett.,* **28,** 1503–1506.

Gruber, A., and A. F. Krueger, 1984: The status of the NOAA outgoing longwave radiation data set. *Bull. Amer. Meteor. Soc.,* **65,** 958–962.

Hastenrath, S., 1995: *Climate Dynamics of the Tropics.* Kluwer, 488 pp.

Hodges, K. I., and C. D. Thorncroft, 1997: Distribution and statistics of African mesoscale convective weather systems based on the ISCCP METEOSAT imagery. *Mon. Wea. Rev.,* **125,** 2821–2837.

Janicot, S., 1992: Spatiotemporal variability of West African rainfall. Part I: Regionalizations and typings. *J. Climate,* **5,** 489–497.

——, and B. Sultan, 2001: Intra-seasonal modulation of convection in the West African monsoon. *Geophys. Res. Lett.,* **28,** 523–526.

——, S. Trzaska, and I. Poccard, 2001: Summer Sahel-ENSO teleconnection and decadal time scale SST variations. *Climate Dyn.,* **18,** 303–320.

Kalnay, E., and Coauthors, 1996: The NCEP/NCAR 40-Year Reanalysis Project. *Bull. Amer. Meteor. Soc.,* **77,** 437–471.

Kiladis, G. N., and K. M. Weickmann, 1997: Horizontal structure and seasonality of large-scale circulations associated with submonthly tropical convection. *Mon. Wea. Rev.,* **125,** 1997–2013.

Laing, A. G., and J. M. Fritsch, 1993: Mesoscale convective complexes in Africa. *Mon. Wea. Rev.,* **121,** 2254–2263.

——, and ——, 1997: The global population of mesoscale convective complexes. *Quart. J. Roy. Meteor. Soc.,* **123,** 389–405.

Lamb, P. J., 1978a: Large scale tropical surface circulation patterns associated with Subsaharan weather anomalies. *Tellus,* **30,** 240–251.

——, 1978b: Case studies of tropical Atlantic surface circulation patterns during recent sub-Saharan weather anomalies: 1967 and 1968. *Mon. Wea. Rev.,* **106,** 482–491.

Le Barbé, L., T. Lebel, and D. Tapsoba, 2002: Rainfall variability in West Africa during the years 1950–90. *J. Climate,* **15,** 187–202.

Liebmann, B., and C. A. Smith, 1996: Description of a complete

(interpolated) outgoing longwave radiation dataset. *Bull. Amer. Meteor. Soc.*, **77,** 1275–1277.

Mathon, V., and H. Laurent, 2001: Life cycle of Sahelian mesoscale convective cloud systems. *Quart. J. Roy. Meteor. Soc.*, **127,** 377–406.

Matthews, A. J., 2002: Intraseasonal variability over West Africa. Preprints, *25th Conf. on Hurricanes and Tropical Meteorology,* San Diego, CA, Amer. Meteor. Soc., 652–653.

Newell, R. E., and J. E. Kidson, 1984: African mean wind changes between Sahelian wet and dry periods. *J. Climatol.*, **4,** 27–33.

Persson, A., 1984: The use of spectrally filtered products in medium-range weather forecasting. ECMWF Tech. Memo. 90, Reading, United Kingdom, 47 pp.

Poccard, I., S. Janicot, and P. Camberlin, 2000: Comparison of rainfall structures between NCEP/NCAR reanalysis and observed data over tropical Africa. *Climate Dyn.*, **16,** 897–915.

Redelsperger, J. L., A. Diongue, A. Diedhiou, J. P. Ceron, M. Diop, J. F. Gueremy, and J. P. Lafore, 2002: Multi-scale description of a Sahelian synoptic weather system representative of the West African monsoon. *Quart. J. Roy. Meteor. Soc.*, **128,** 1229–1257.

Reed, R. J., D. C. Norquist, and E. E. Recker, 1977: The structure and properties of African wave disturbances as observed during Phase III of GATE. *Mon. Wea. Rev.*, **105,** 317–333.

Roca, R., C. Piriou, J. P. Lafore, and J. L. Redelsperger, 2002: Extra-tropical dry air intrusions in the West African monsoon region. Preprints, *25th Conf. on Hurricanes and Tropical Meteorology,* San Diego, CA, Amer. Meteor. Soc., 277–278.

Rowell, D. P., 2001: Teleconnections between the tropical Pacific and the Sahel. *Quart. J. Roy. Meteor. Soc.*, **127,** 1683–1706.

——, C. K. Folland, K. Maskell, and M. N. Ward, 1995: Variability of summer rainfall over Tropical North Africa (1906–1992): Observations and modelling. *Quart. J. Roy. Meteor. Soc.*, **121,** 669–704.

Scavuzzo, C. M., M. A. Lamfri, H. Teitelbaum, and F. Lott, 1998: A study of the low-frequency inertio-gravity waves observed during the Pyrenees Experiment. *J. Geophys. Res.*, **103** (D2), 1747–1758.

Sow, C. S., 1997: Diurnal rainfall variations in Senegal. *Secheresse,* **8,** 157–162.

Sultan, B., and S. Janicot, 2000: Abrupt shift of the ITCZ over West Africa and intra-seasonal variability. *Geophys. Res. Lett.*, **27,** 3353–3356.

——, ——, and A. Diedhiou, 2003: West African monsoon dynamics. Part II: The ''pre-onset'' and the ''onset'' of the summer monsoon. *J. Climate,* **16,** 3407–3427.

Taylor, C. M., and T. Lebel, 1998: Observational evidence of persistent convective-scale rainfall patterns. *Mon. Wea. Rev.*, **126,** 1597–1607.

——, F. Saïd, and T. Lebel, 1997: Interactions between the land surface and mesoscale rainfall variability during HAPEX-Sahel. *Mon. Wea. Rev.*, **125,** 2211–2227.

Ward, M. N., 1998: Diagnosis and short-lead time prediction of summer rainfall in tropical North Africa at interannual and multidecadal timescales. *J. Climate,* **11,** 3167–3191.